On-Line Monitoring of a Crystallization Process

Patricia Mougin, Alistair Thomas, Derek Wilkinson, and Graeme White
Center for Molecular and Interface Engineering, Dept. of Mechanical and Chemical Engineering, Heriot-Watt University, Riccarton, Edinburgh EH14 4AS, U.K.

Kevin J. Roberts
Institute for Particle Science and Engineering, Dept. of Chemical Engineering, University of Leeds, Leeds LS2 9JT, U.K.

Norbert Herrmann, Robert Jack, and Richard Tweedie
Malvern Instruments Ltd., Enigma Business Park, Malvern, Worcestershire, WR14 1XZ, U.K.

The application of ultrasonic spectroscopy for particle-size measurements was investigated during the batch crystallization of (L)-glutamic acid α-polymorph from an aqueous solution. The technique, based on measurements of the attenuation of ultrasonic waves through the suspension, was applied using a prototype ultrasonic spectrometer with a flow-through cell. High-precision measurements of ultrasonic attenuation in the frequency range 7–110 MHz were performed, the deconvolution of which enabled in-process measurement of crystal size distribution and solid concentration throughout the crystallization process. In addition to evincing secondary nucleation, growth and crystal breakage on-line in real time, the experimental results were used to obtain kinetic parameters essential for process design, including secondary nucleation rate and growth rate.

Introduction

Crystallization is an important unit operation for the production of solid products, and batch crystallization processes are commonplace in the speciality chemicals and pharmaceuticals industry. The nonlinearity of process variables during batch crystallization requires on-line techniques to measure these variables. The control of crystal-size distribution (CSD) in particular is important, as it is a major driver dictating product behavior downstream through its impact on unit operations such as filtration, drying, transport, and storage. However, on-line measurement and control of CSD can be problematic, particularly because most commercially available particle sizing methods rely on optical techniques which are inherently not suited for examining suspensions at solid concentrations typical of a batch crystallization process.

This work presents a study on the feasibility of on-line crystal size and concentration measurements by ultrasonic attenuation spectroscopy, and follows a successful study of the application of this technique for *in situ* measurements (Mougin et al., 2002). In this study, (L)-glutamic acid was crystallized under solvent and cooling rate conditions to produce the polymorphic form α. The α-form of (L)-glutamic acid has a distinctive prismatic morphology illustrated by the microscope image presented in Figure 1.

Correspondence concerning this article should be addressed to P. Mougin at this current address: SSCI, Inc., 3065 Kent Avenue, West Lafayette, IN 47906.
Current address of R. Tweedie: Hasbro Europe, Technology Development, 2 Roundwood Ave., Stockley Park, Uxbridge UB11 1AZ, U.K.

Ultrasonic Spectroscopy and Crystallization Process

Ultrasonic spectroscopy: background

Ultrasonic attenuation spectroscopy is a comparatively new characterization technique, which is suitable for measurement of particle sizes within the approximate range 0.01 μm–1,000 μm for slurries of solid concentration in the range 0.1 vol. %–50 vol. % (Alba, 1992; Pendse and Sharma, 1993). It is capable of examining concentrated or optically opaque systems without the need for analyte dilution and, therefore,

is attracting some attention as a potentially useful technique for characterizing many particulate suspensions of practical importance.

The deconvolution of ultrasonic attenuation was performed using the mathematical model of Epstein and Carhart (1953) and Allegra and Hawley (1972) (ECAH model), which predicts the attenuation of a sound wave when passing through a suspension. Due to the variety of mechanisms by which an acoustic wave may be attenuated through a suspension (scattering, visco-inertial, and thermal scattering), a comprehensive description of the mechanisms necessitates a set of physical parameters describing solid and liquid phases: density, speed of sound, heat capacity, thermal conductivity, thermal expansion coefficient, viscosity (liquid phase), shear rigidity (solid particles), and sound attenuation. In practice, however, it was found that only a subset of these physical parameters needs to be known accurately. The remaining physical properties may be estimated with sufficient accuracy for reliable data inversion in the case of inorganic (Babick et al., 2000) and organic crystals (Mougin, 2001).

Physical characterization of liquid medium and solid particles

This work follows on from a study of the measurement technique for crystallization applications in which a procedure was devised to measure particle-size distributions in the case of crystallizing suspensions. This procedure consists of calibration experiments, in which ultrasonic attenuation is measured through undersaturated solutions at various conditions of solute concentration and temperature, enabling the retrieval of CSD parameters as solid content and solute concentration evolve during the crystallization process (Mougin, 2001; Mougin et al., 2001).

Due to the low solute concentration at which the crystallization experiments were carried out, the influence of solute concentration on the liquid medium was considered to be negligible for all physical properties characterizing the liquid phase. The influence of temperature on the attenuation spectrum of the liquid medium was measured between 35°C and 50°C, and was extrapolated to 15°C. The physical properties describing liquid and solid phases are summarized in Table 1.

Experimental Methods

Experimental setup

A prototype instrument equipped with a flow-through cell was developed for this project in conjunction with Malvern Instruments Ltd. The 470 mL stainless steel flow-through cell, as well as the tubing of the pumping line were jacketted to maintain the cell temperature at the reactor temperature. The temperature of the tubing and cell jackets was set by a thermostatic bath (Haake F3), controlled by a temperature programmer (Haake PG20) allowing linear cooling. The spectrometer's flow-through cell was connected to the side ports of a double-jacketted 2.6 L glass reaction calorimeter (HEL Ltd. Oil for temperature control was circulated through the inner jacket, while the outer vacuum jacket provided thermal insulation from the outside environment. The agitator was a 6-pitched-blade impeller and the solution was kept agitated at 200 rpm. Circulating oil temperature and agitator speed were controlled by a control and data acquisition unit (HEL Ltd) linked to a desktop PC. The temperature of the crystallizing solution, solution turbidity, and temperature of oil into and from the inner jacket were recorded every 20 s. The oil temperature was adjusted by the PC/control system to achieve a linear cooling rate. The turbidity of the solution/slurry was measured using a turbidometric fiber optic probe which was developed in-house.

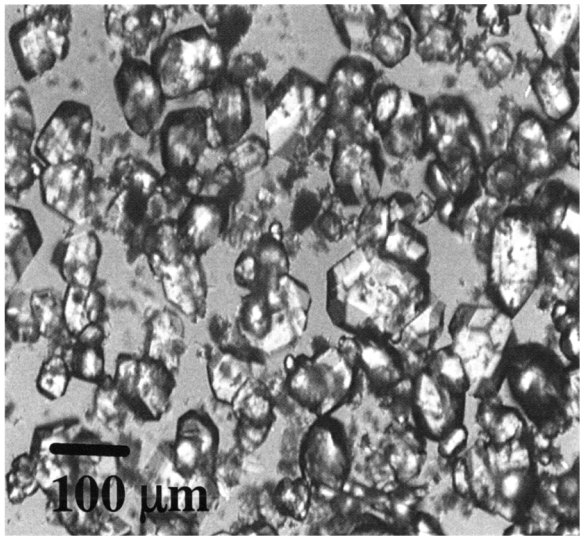

Figure 1. Microscope image of α-(L)-glutamic acid crystals grown by fast cooling from aqueous solution.

For the development of the on-line ultrasonic particle sizing technique, an experimental procedure was developed to

Table 1. Physical Parameters of (*L*)-Glutamic Acid Crystals and a 2 wt. % Aqueous Solution of (L)-glutamic Acid

Property	(L)-glutamic Acid Crystal	2 wt. % Aqueous Solution of (L)-glutamic acid
Density ($kg \cdot m^{-3}$)	1.54×10^3	1.00×10^3
Sound Speed ($m \cdot s^{-1}$)	4.07×10^3	1.480×10^3
Thermal Dilation (K^{-1})	2×10^{-5}	2.6×10^{-4}
Thermal Conductivity ($J \cdot m^{-1} \cdot s^{-1} \cdot K^{-1}$)	4.2×10^{-1}	5.95×10^{-1}
Heat Capacity ($J \cdot kg^{-1} \cdot K^{-1}$)	1.24×10^3	4.18×10^3
Shear Rigidity ($N \cdot m^{-2}$)	8×10^9	
Viscosity ($N \cdot s \cdot m^{-2}$)		1.0×10^{-3}
Attenuation ($dB \cdot m^{-1}$)	$4 \times 10^{-4} \cdot f^2$	$(8.063 \times 10^{-3} - 5.5 \times 10^{-5} \cdot T) \cdot f^2$

*Acoustic attenuation measured at temperature T in °C, frequency f in MHz.

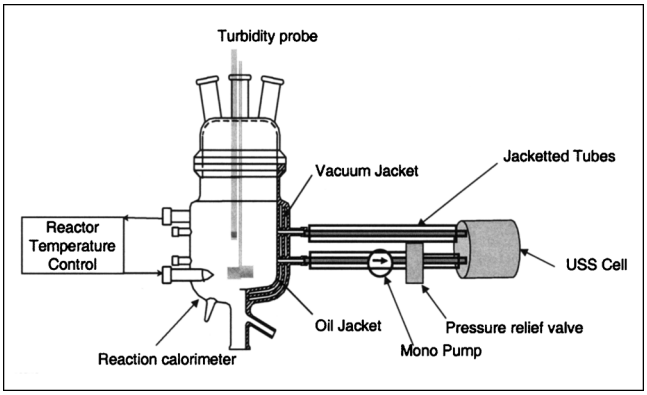

Figure 2. Experimental setup.

pump the crystallizing solution continuously through the prototype on-line ultrasonic spectrometer. In selecting the pump, one of the most important considerations was that the pumping action should not damage the crystals, nor should it involve a pulsed discharge which could potentially interfere with the acoustic signals. A Mono progressive cavity screw pump (George Meller Ltd) was selected used at a flow rate of 1 L/min. Pinch values mounted on silicon tubing were used as on/off valves at the reaction calorimeter ports. A pressure relief connected to the Mono pump was designed to stop the pump in case of blockage. The experimental setup is presented in Figure 2.

Materials and methods

Aqueous solutions were prepared with distilled water. (L)-glutamic acid was purchased from Aldrich. Experiments on crystallization of (L)-glutamic acid were carried out by cooling an aqueous solution at 35 g/1,000 g of water at 0.2°C/min from 75°C down to 20°C, in order to obtain the α-form of (L)-glutamic acid. The nature of the crystal form was determined by on-line XRD.

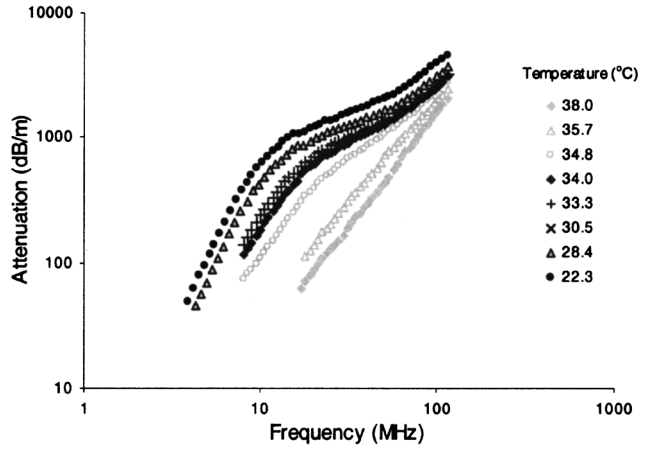

Figure 3. Evolution of attenuation spectra recorded during the crystallization of (L)-glutamic acid from an aqueous solution at 35 g/1,000 g of water cooling at 0.2°C/min from 75°C down to 20°C.
The legend indicates the temperature expressed in °C.

Experimental Results

Figure 3 is an example of evolution of attenuation spectra recorded during the crystallization of (L)-glutamic acid α-form under the conditions mentioned above. It can be seen that the spectra obtained were of good quality as shown by their lack of irregularities. Experiments were repeated to confirm the results. Size analysis was carried out using these spectra. Figure 4 shows the evolution of the CSD, the detail of which can be found in Table 2.

Figure 4a shows the growth of the particles, illustrated by the shift of the distribution towards the bigger sizes. It can be seen from Figure 4b that, following this period of growth, a shoulder appears in the distribution in the smaller sizes and this becomes more pronounced as the crystallization process evolves. This shoulder can *a priori* be attributed either to nucleation or to attrition and crystal breakage. A closer look at the higher limit of the distribution shows a narrowing in the bigger sizes simultaneous with the appearance of the shoulder at smaller sizes, which is consistent with crystal breakage and attrition. Indeed, attrition fragments may be the source of new nuclei for secondary nucleation.

Discussion

Evolution of solid concentration and CSD

Figure 5 shows the evolution of mean size (D_{50}) and solid concentration during the crystallization of (L)-glutamic acid

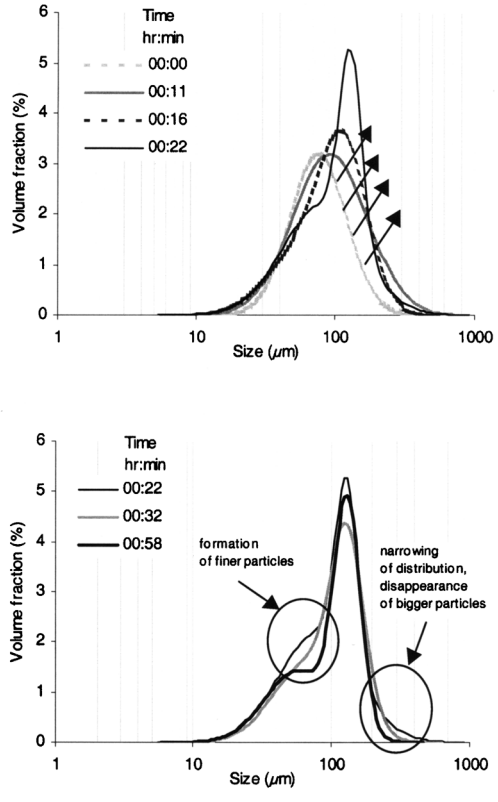

Figure 4. Evolution of the CSD measured during crytallization of (L)-glutamic acid from an aqueous solution at 35 g/1,000 g of water cooling at 0.2°C/min from 75°C down to 20°C (origin of time when solid concentration > 0.1 vol. %).

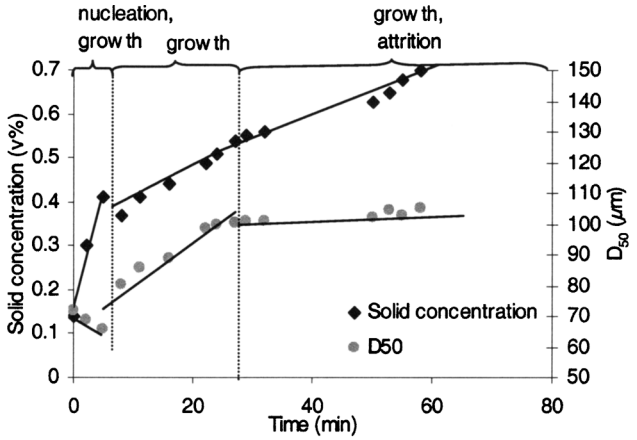

Figure 5. Evolution of size and solid concentration during the crystallization of (L)-glutamic acid from an aqueous solution at 35 g/1,000 g water, cooling down at 0.2°C/min (origin of time when solid concentration > 0.1 vol. %).

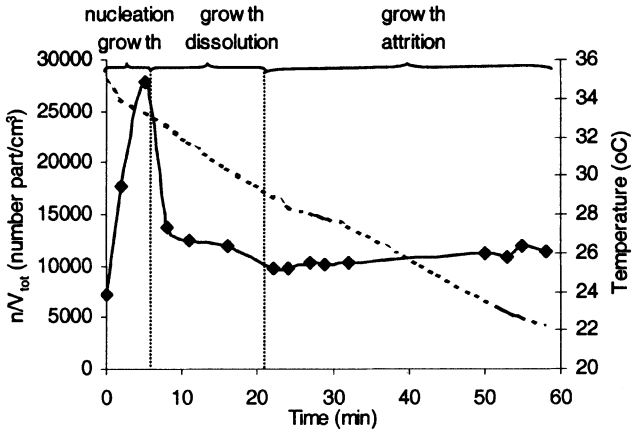

Figure 6. Evolution of the average number of particles per unit volume during the cooling crystallization of (L)-glutamic acid from a 3.5 wt. % aqueous solution, cooling down at 0.2°C/min (cooling profile in dotted line).

α-form. Three stages can be seen: (1) Rapid increase of solid concentration and decrease of size; (2) Slower increase of solid concentration with increase of size; and (3) Increase of solid concentration at constant size.

These observations should also be seen in conjunction with the CSD analyses presented in the previous section and may be interpreted as follows:

- In stage 1, the average size decreases, in spite of the slight growth of the main part of the distribution, as a result of nucleation generating very small particles. This period is accompanied by a high solid mass increase rate due to the formation of new nuclei.
- In stage 2, the mass increase rate is lower and the crystal size increases. This corresponds to a period of crystal growth, with low or no nucleation or crystal breakage.
- In stage 3, the crystal growth comes to a halt, whereas the mass increase rate remains almost identical to that observed in stage 2. The slight difference may be due to the gradual reduction of supersaturation during stages 2 and 3.

In summary, the data is consistent with the following phase structure:

- nucleation and growth (stage 1);
- growth and attrition, with the growth rate being higher than the attrition rate (stage 2); and
- growth and attrition, the growth and attrition rates of large particles being of the same order of magnitude (stage 3).

This interpretation can be supported further by calculation of the number concentration of particles (average number of particles per unit volume) n_{ave}/V_{tot}

$$\frac{n_{ave}}{V_{tot}} = \frac{6C_s}{\pi \overline{L}^3} \tag{1}$$

where C_s is the solid concentration, and the average size $\overline{L}$ was taken equal to the median diameter of the distribution.

Figure 6 shows the evolution with time of n_{ave}/V_{tot} during the crystallization process. It is seen that stage 2, which was

Table 2. Evolution of CSD During the Cooling Crystallization of (L)-Glutamic Acid α-Polymorph*

Stage	T (°C)	Time (min)	C (vol. %)	D_{50} (μm)	dD_{50}/dt(m/s)	G_a (m/s)
	34.8	0	0.14	71.7		1.5×10^{-7}
1	34.0	2	0.3	68.6		7.7×10^{-8}
	33.3	5	0.41	65.6		5.5×10^{-8}
	32.6	8	0.37	80.2		7.7×10^{-9}
	31.8	11	0.41	85.7		7.4×10^{-9}
2	30.4	16	0.44	88.9	$(2.6\pm0.4)\times10^{-8}$	8.8×10^{-9}
	29.0	22	0.49	98.6		8.7×10^{-9}
	28.4	24	0.51	99.8		$8.5\times10^{10-9}$
	28.1	27	0.54	100.1		6.3×10^{-9}
	27.8	29	0.55	101.2		6.1×10^{-9}
	27.4	32	0.56	101.0		6.0×10^{-9}
3	23.6	50	0.63	102.2	$(2.3\pm0.3)\times10^{-9}$	5.3×10^{-9}
	23.0	53	0.65	104.8		5.3×10^{-9}
	22.7	55	0.68	102.8		5.0×10^{-9}
	22.3	58	0.7	105.3		4.9×10^{-9}

*From an aqueous solution at 35 g/1,000 g of water, cooling at 0.2°C/min from 75°C down to 20°C down to 15°C.

postulated to be a period of growth for which size and solid concentration increase, is accompanied by a decrease of the total number of particles. This stage may be seen as a transition period, during which small nuclei/particles resulting from the nucleation period is stage 1 may dissolve while the bigger crystals grow (Ostwald ripening). During stage 3, a small increase of the average number of particles occurs, consistent with a period of attrition.

Growth rates

The combination of solid concentration data with size data is convenient as it allows observations of phenomena such as nucleation or attrition and their quantification in some cases. Two different approaches may be adopted to give estimates of growth rate during the crystallization of (L)-glutamic acid. The first approach, based on the size increase as monitored from the CSD data, relates to the size of the entire crystal population and is likely to be less sensitive to the formation of small particles via nucleation or attrition, provided that large particles are already present in suspension. The second approach, based on the solid content in suspension is a global method that does not allow any distinction between the various mechanisms by which solid content may increase during crystallization, that is, the effects of nucleation, attrition, dissolution, or growth are monitored together. The determination of growth rate under these conditions cannot be done without a set of assumptions relative to the process. Using these two tools conjointly, it is possible to determine some important parameters.

Linear trends were fitted to size data (D_{50}) measured after the initial nucleation period in order to estimate the growth rate, giving a growth rate equal to $(2.6\pm0.4)\times10^{-8}$ m/s in stage 2 and $(2.3\pm0.3)\times10^{-9}$ m/s in stage 3. It is clear that this method does not allow the detection of rapid changes of growth rates as the size of the ensemble of the crystal population is monitored. Linear trends were also fitted to concentration data at each stage of the crystallization process. The following relationships were used

$$\text{Stage 1: } C_1(t) = (0.053(\pm0.012))\times t + 0.16(\pm0.04) \quad (2)$$

$$\text{Stage 2: } C_2(t) = (0.0064(\pm0.0013))\times t + 0.346(\pm0.021) \quad (3)$$

$$\text{Stage 3: } C_3(t) = (0.0049(\pm0.0003))\times t + 0.40(\pm0.01) \quad (4)$$

where the solid volume concentration C and the time t are expressed in vol. and min, respectively.

Assuming that nucleation occurs mainly in stage 1 and that the growth rate remains unchanged from stage 1 to stage 2 allows estimation of the level of nucleation during stage 1 from solid concentration data. The difference $\rho_s\times[(dC/dt|_1) - (dC/dt|_2)]$ is a direct measure of the nucleation rate in units of weight of solute per unit volume of solvent and per unit time (where ρ_s is the density of the crystal and C the solid volume concentration). Nucleation rate was thus estimated to be equal to $(1.2\pm0.3)\times10^{-5}$ g/(cm$^3\cdot$s).

Furthermore, assuming a spherical shape for the secondary nuclei, the size of the nuclei can be estimated since a measure of the solute involved in each secondary nucleation event is known, along with the number of particles involved. The volume V_s of particles involved in secondary nucleation at $t = t_1$, the time of transition from stage 1 to stage 2, is

$$V_s = V_{\text{tot}}\left[C_1(t_1) - C_1(t_0) - \left.\frac{dC}{dt}\right|_2 \times (t_1 - t_0)\right] \quad (5)$$

and the number of particles involved in secondary nucleation is

$$N_s = n(t_1) - n(t_0) \quad (6)$$

where $t_0 = 0$ is the initial time.

Thus, the average size $\overline{L}_{\text{nuc}}$ of the secondary nuclei is

$$\overline{L}_{\text{nuc}} = \sqrt[3]{\frac{6V_s}{\pi.N_s}} \quad (7)$$

giving $\overline{L}_{\text{nuc}} = 1.0\pm0.1$ μm.

This result is in good agreement with estimations of the size of secondary nuclei reported in the literature, typically in the range of 1–10 μm (Garside et al., 1979), whereas smaller nuclei are unlikely to survive in an agitated crystallizer where fluctuations of both temperature and supersaturation occur (Garabedian and Strickland-Constable, 1972). This is confirmed by the disappearance of particles in stage 2, as shown in Figure 6.

In the absence of nucleation or dissolution, that is, at fixed particle number concentration, the overall mass growth rate R_G (mass deposition rate per unit crystal surface area) may be calculated from the correlation of solid concentration and size data as follows

$$R_G = \frac{\rho_s\cdot\overline{L}}{6C_s}\times\frac{dC_s}{dt} \quad (8)$$

where ρ_s is the solid density, $\overline{L}$ is the surface mean diameter, C_s is the solid volume fraction, and t is the time.

The overall mass growth rate may be translated into overall linear growth rate G as follows

$$G = \frac{\beta}{3\alpha\cdot\rho_s}\times R_G \quad (9)$$

where α and β are the volume and surface shape factor, respectively.

While nucleation may be easily observed at the beginning of the crystallization (stage 1), the combination of various phenomena (growth, attrition/secondary nucleation, and possibly dissolution) makes it impossible to distinguish one from the other. For this reason, the overall rates calculated from Eqs. 8 and 9 will be called *apparent* growth rates $R_{G,a}$ and G_a, and may include mass variations due to dissolution and secondary nucleation.

Calculated values of apparent overall linear growth rate G_a are listed with the results in Table 2, along with the values of the growth rate as determined from the size data. Comparing

dD_{50}/dt obtained from size data with G_a shows that G_a becomes less than dD_{50}/dt immediately after the end of stage 1. This may be attributed to dissolution, and is consistent with the decrease of the total number of particles at the end of stage 1, which was observed in Figure 6.

Although the attrition in stage 3 should not cause mass variations directly, it may involve modification of the parent crystal's surface which can induce heterogeneous nucleation. The higher value of G_a compared to dD_{50}/dt in stage 3 could, therefore, be explained by further nucleation as a result of attrition.

Finally, it is interesting to note the slight change of slope of solid concentration between stages 2, and also the decrease in G_a at that point. This decrease may be the result of the decrease of supersaturation level or, alternatively, may be due to a variation of the overall growth rate due to a slower growth rate of the attrition fragments.

Conclusions

Good experimental results were obtained using this new experimental setup enabling on-line ultrasonic measurements of quality comparable to *in situ* measurements. Although minor problems of crystal breakage were encountered, the experimental setup proved to be well-behaved and reliable. In addition to enabling the observation of nucleation, growth, and crystal breakage on-line and in real time, this new experimental setup was used to estimate kinetic parameters essential for process design, including secondary nucleation rate and growth rate.

Acknowledgments

This work has been carried out as part of the Chemicals Behaving Badly initiative, a collaborative project funded by EPSRC grant GR/L/68797, together with industrial support from AstraZeneca, BASF, GlaxoSmithKline, ICI, Malvern Instruments Ltd., Pfizer, and Syngenta. We gratefully acknowledge Pr. Leslie Ford for his input in this project, and Dr. Will Wood from Syngenta for providing us with some of the physical properties of (L) glutamic acid. We also acknowledge all other members of this academic/industrial team for their contribution to the overall project.

Literature Cited

Alba, F., "Method and Apparatus for Determining Particle Size Distributions and Concentration in a Suspension using Ultrasonics," U.S. Patent No. 5,121,629 (June 16, 1992).

Allegra, J. R., and S. A. Hawley, "Attenuation of Sound in Suspensions and Emulsions: Theory and Experiments," *J. of Acoust. Soc. of Amer.*, **51**, 1545 (1972).

Babick, F., F. Hinze, and S. Ripperger, "Dependence of Ultrasonic Attenuation on the Material Properties," *Coll. Surf. A: Physicochem. and Eng. Aspects*, **172**, 33 (2000).

Epstein, P. S., and R. R. Carhart, "The Absorbtion of Sound in Suspensions and Emulsions: 1. Water Fog in Air," *J. of Acoust. Soc. of Amer.*, **25**, 553 (1953).

Garabedian, H., and R. F. Strickland-Constable, "Collision Breeding of Crystal Nuclei: Sodium Chlorate. I," *J. of Crystal Growth*, 13/14, 506 (1972).

Garside, J., I. T. Rusli, and M. A. Larson, "Origin and Size Distribution of Secondary Nuclei," *AIChE J.*, **25**, 57 (1979).

Mougin, P., "In situ and On-Line Ultrasonic Attenuation Spectroscopy for Particle Sizing during the Crystallization of Organic Fine Chemicals," PhD Thesis, Heriot-Watt University, Edinburgh, U.K. (2001).

Mougin, P., K. J. Roberts, R. Tweedie, and D. Wilkinson, "An Examination of the in-situ Measurement of Particle Size and Its Distribution Using Ultrasonic Attenuation Spectroscopy during the Crystallization of Organic Fine Chemical Products," *J. of Acoust. Soc. of Amer.*, **109**, 274 (2001).

Mougin, P., D. Wilkinson, and K. J. Roberts, "In Situ Measurement of Particle Size during the Crystallization of L-Glutamic Acid under Two Polymorphic Forms: Influence of Crystal Habit on Ultrasonic Attenuation Measurements," *Crystal Growth and Design*, **2**, 227 (2002).

Pendse, H. P., and A. Sharma, "Particle-Size Distribution Analysis of Industrial Colloidal Slurries using Ultrasonic Spectroscopy," *Particle & Particle Systems Characterization*, **10**, 229 (1993).

Manuscript received Jan. 28, 2002, and revision received Sept. 12, 2002.